



Structural and magnetic properties of Mg-Zn ferrites ($\text{Mg}_{1-x}\text{Zn}_x\text{Fe}_2\text{O}_4$) prepared by sol-gel method



Pamela Yajaira Reyes-Rodríguez^{a,*}, Dora Alicia Cortés-Hernández^a,
 José Concepción Escobedo-Bocardo^a, José Manuel Almanza-Robles^a,
 Héctor Javier Sánchez-Fuentes^a, Argentina Jasso-Terán^a, Laura Elena De León-Prado^a,
 Juan Méndez-Nonell^b, Gilberto Francisco Hurtado-López^c

^a Cinvestav-Unidad Saltillo, Av. Industrial Metalúrgica #1062, Parque Industrial Saltillo-Ramos Arizpe, CP 25900, México

^b Centro de Investigación en Materiales Avanzados, Ave. Miguel Cervantes #120, Complejo Industrial Chihuahua, CP 31109 Chihuahua, México

^c Centro de Investigación en Química Aplicada, Blvd. Enrique Reyna Hermosillo #140, CP 25294 Saltillo, Coahuila, México

ARTICLE INFO

Keywords:

Mg-Zn ferrite
 Sol-gel
 Magnetic properties
 Heating ability

ABSTRACT

In this study, the $\text{Mg}_{1-x}\text{Zn}_x\text{Fe}_2\text{O}_4$ nanoparticles ($x=0-0.9$) were prepared by sol-gel method. These ferrites exhibit an inverse spinel structure and the lattice parameter increases as the substitution of Zn^{2+} ions is increased. At lower Zn content ($0.1 \leq x \leq 0.5$), saturation magnetization (M_s) increases, while it decreases at higher Zn content ($x \geq 0.6$). The remnant magnetization (0.17–2.0 emu/g) and coercive field (6.0–60 Oe) indicate a ferrimagnetic behavior. The average core diameter of selected ferrites is around 15 nm and the nanoparticles morphology is quasi spherical. The heating ability of some $\text{Mg}_{0.9}\text{Zn}_{0.1}\text{Fe}_2\text{O}_4$ and $\text{Mg}_{0.7}\text{Zn}_{0.3}\text{Fe}_2\text{O}_4$ aqueous suspensions indicates that the magnetic nanoparticles can increase the medium temperature up to 42 °C in a time less than 10 min

1. Introduction

Magnetic nanoparticles with a general formula of MFe_2O_4 ($\text{M}=\text{Fe}, \text{Mn}, \text{Zn}, \text{Mg}, \text{Co}, \text{Ca}$) have been studied for biomedical applications due to their biocompatibility, chemical stability under physiological conditions and superparamagnetic properties [1,2]. The incorporation of magnesium ions into the spinel structure of iron oxide leads to a magnetic magnesium ferrite (MgFe_2O_4) that possesses thermal and chemical stability and improved electric and magnetic properties compared to the bulk material [3]. Magnesium ferrite nanoparticles are used in a wide variety of applications, including heterogeneous catalysis, sensors, magnetic technologies and biomedicine. This ferrite has an inverse spinel structure and shows a ferrimagnetic behavior. In addition, it has been investigated as a potential candidate for the cancer treatment by hyperthermia therapy due to its appropriate biocompatibility and heating ability [3]. Kassabova et al. [4] reported the synthesis of Mg-Zn ferrites by a citrate method followed by heat treatment at 450 or 1200 °C. They obtained ferrites with a single spinel crystalline structure and the crystallite size was in a range within 5 and 8 nm, however the particle size was not evaluated. Kassabova et al. [4] reported that these ferrites can be suitable for hyperthermia

applications, nonetheless the heating ability of these materials was not evaluated. The substitution of Mg ions by non-magnetic ions such as Zn^{2+} , Ca^{2+} , Ti^{4+} , Zr^{4+} , Al^{3+} , etc., into a magnesium ferrite structure may increase M_s value due to the increase in the net magnetic moment between Fe and Mg ions [5,6]. This work reports the synthesis of $\text{Mg}_{1-x}\text{Zn}_x\text{Fe}_2\text{O}_4$ (with $x=0.0-0.9$) nanoparticles by the sol-gel method and the effect of zinc incorporation on the crystalline structure, magnetic properties and heating ability of the obtained materials for their potential use as thermoseeds in hyperthermia treatment.

2. Materials and methods

The $\text{Mg}_{1-x}\text{Zn}_x\text{Fe}_2\text{O}_4$ ($x=0.0-0.9$) ferrites were prepared by sol-gel method according to the stated in the literature [7] and using $\text{Fe}(\text{NO}_3)_3 \cdot 9\text{H}_2\text{O}$, $\text{Mg}(\text{NO}_3)_2 \cdot 6\text{H}_2\text{O}$, $\text{Zn}(\text{NO}_3)_2 \cdot 6\text{H}_2\text{O}$ in a molar ratio of 2:1 (Fe:Mg-Zn) and ethylene glycol ($\text{C}_2\text{H}_6\text{O}_2$) as reaction medium. The obtained powder were heat treated at 500 °C for 60 min. Synthesized nanoparticles were characterized by X-ray diffraction (XRD, X'pert, Philips 3040), Fourier transform-Infrared spectroscopy (FT-IR, Nicolet Gemini, 550 C) and transmission electron microscopy-energy dispersive spectroscopy (TEM-EDS Titan 80-300) for the determination of

* Corresponding author.

E-mail address: pamela2244_4@hotmail.com (P.Y. Reyes-Rodríguez).

<http://dx.doi.org/10.1016/j.jmmm.2016.10.078>

Received 21 June 2016; Received in revised form 13 October 2016; Accepted 16 October 2016

Available online 17 October 2016

0304-8853/ © 2016 Elsevier B.V. All rights reserved.

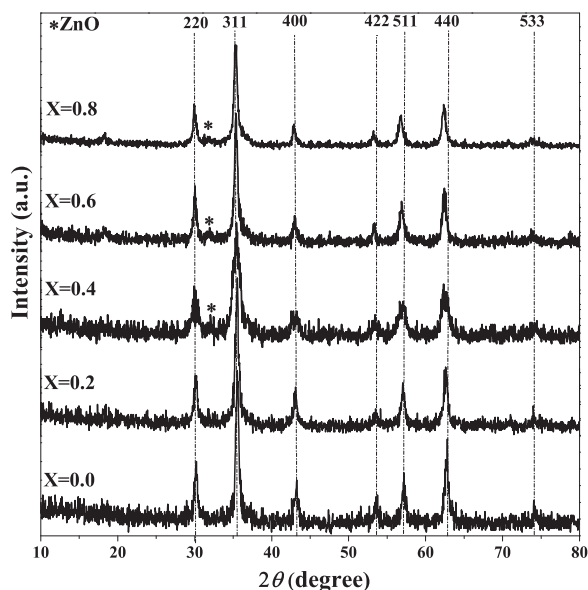


Fig. 1. XRD patterns of $Mg_{1-x}Zn_xFe_2O_4$ samples with $x=0, 0.2, 0.4, 0.6$ and 0.8 of Zn^{2+} .

Table 1
Magnetic properties, crystallite size (D) and lattice parameter (a) of $Mg_{1-x}Zn_xFe_2O_4$ ($x=0-0.9$ of Zn^{2+}) samples.

| Sample | M_s (emu/g) | M_r (emu/g) | H_c (Oe) | D (nm) | a (Å) |
|---------------------------|---------------|---------------|------------|----------|---------|
| $Mg_{1.0}Zn_0Fe_2O_4$ | 27.81 | 0.47 | 9 | 18 | 8.374 |
| $Mg_{0.9}Zn_{0.1}Fe_2O_4$ | 38.45 | 0.98 | 42 | 17 | 8.374 |
| $Mg_{0.8}Zn_{0.2}Fe_2O_4$ | 39.21 | 0.56 | 20 | 17 | 8.363 |
| $Mg_{0.7}Zn_{0.3}Fe_2O_4$ | 42.22 | 0.49 | 6 | 18 | 8.332 |
| $Mg_{0.6}Zn_{0.4}Fe_2O_4$ | 42.85 | 2.00 | 45 | 20 | 8.386 |
| $Mg_{0.5}Zn_{0.5}Fe_2O_4$ | 42.33 | 0.40 | 10 | 19 | 8.403 |
| $Mg_{0.4}Zn_{0.6}Fe_2O_4$ | 38.07 | 0.62 | 10 | 19 | 8.415 |
| $Mg_{0.3}Zn_{0.7}Fe_2O_4$ | 26.41 | 1.61 | 28 | 17 | 8.415 |
| $Mg_{0.2}Zn_{0.8}Fe_2O_4$ | 18.61 | 1.10 | 60 | 20 | 8.415 |
| $Mg_{0.1}Zn_{0.9}Fe_2O_4$ | 15.57 | 0.17 | 17 | 22 | 8.432 |

the crystalline structure, size and morphology. The magnetic parameters of saturation magnetization (M_s), remnant magnetization (M_r) and coercive field (H_c) were measured by vibrating sample magnetometry (VSM, Quantum Design, 6000) at room temperature and 12 kOe using powder samples. The heating capacity was evaluated by solid state magnetic induction for 10 min (Ambrell, Easy Heat 0224, 10.2 kA/m, 354 kHz) using suspensions of 2.0, 4.0, 6.0, 8.0, and 10.0 mg of ferrite per mL of deionized water. The heating efficiency, specific absorption rate, (SAR) was calculated by direct calorimetric

measurement according to Eq. (1) [8–11].

$$SAR = \frac{\Delta T}{\Delta t} * \frac{C}{m} \tag{1}$$

where m is the ferrite mass in the fluid per unit mass of fluid, $\Delta T/\Delta t$ is the slope of the temperature vs time curve and C is the heat capacity of the fluid per unit mass of fluid.

3. Results

The XRD patterns of $Mg_{1-x}Zn_xFe_2O_4$ samples with $x=0, 0.2, 0.4, 0.6$ and 0.8 of Zn^{2+} are shown in Fig. 1. The reflections observed correspond to those of $MgFe_2O_4$ ($x=0$ of Zn^{2+} , JCPDS 88-1935). A slight displacement of these reflections to the left was observed when Mg^{2+} ions are substituted by Zn^{2+} ions. This indicates that the incorporation of Zn into the Mg ferrite is taking place. The displacement is due to the larger ionic radius of Zn (0.82 Å) in comparison to those of Fe (0.67 Å) and Mg (0.66 Å) ions. A secondary phase, ZnO, was detected when the Zn content was higher than 0.4 ($x > 0.4$). Some authors have reported that Zn^{2+} ions located into a spinel ferrite show a strong preference for tetrahedral interstitial sites (A-sites) and can replace both Mg^{2+} and Fe^{3+} ions located in A-sites [12,13].

Measured magnetic parameters (M_s , M_r and H_c), crystallite size calculated by Scherrer equation [14] and lattice parameter of all samples are listed in Table 1. The lattice parameter value increases from 8.37 to 8.43 Å which indicates the incorporation of Mg^{2+} ions into the inverse spinel crystalline structure. Additionally, an increase in M_s is observed as the content of Zn^{2+} increases ($x=0.1$ to 0.5) reaching at maximum value of 42.85 emu/g (emu/g is magnetic moment per mass of magnetic material) for $x=0.4$, while for $x > 0.6$ M_s decreases probably due to the ZnO secondary phase, which was also observed by Hanjarpour et al. [15], and other authors [5,16]. It has been reported in the literature that Zn^{2+} ions can replace Mg^{2+} ions in A-sites, while simultaneously migration of Fe^{3+} ions from A sites to B sites occur, concluding that the variation in M_s is a result of the net magnetic moment between Fe^{3+} ions located into A and B sites [5,15]. As observed M_r and H_c vary with no tendency, which it is usually related to the magnetic anisotropy change as a result of the different possible orderings that can take place during the cations incorporation into the magnetic spinel. According to the magnetic parameters (high M_s , M_r and H_c close to zero), the magnetic behavior (ferrimagnetic state) and the absence of secondary phases (ZnO), $Mg_{0.9}Zn_{0.1}Fe_2O_4$ and $Mg_{0.7}Zn_{0.3}Fe_2O_4$ were selected for further investigation.

In Fig. 2 the hysteresis loops (a) and the FT-IR characterization (b) of selected samples are presented. From the hysteresis loops and the M_r and H_c values it is possible to confirm that the synthesized samples show a ferrimagnetic behavior. According to the FT-IR spectra, the

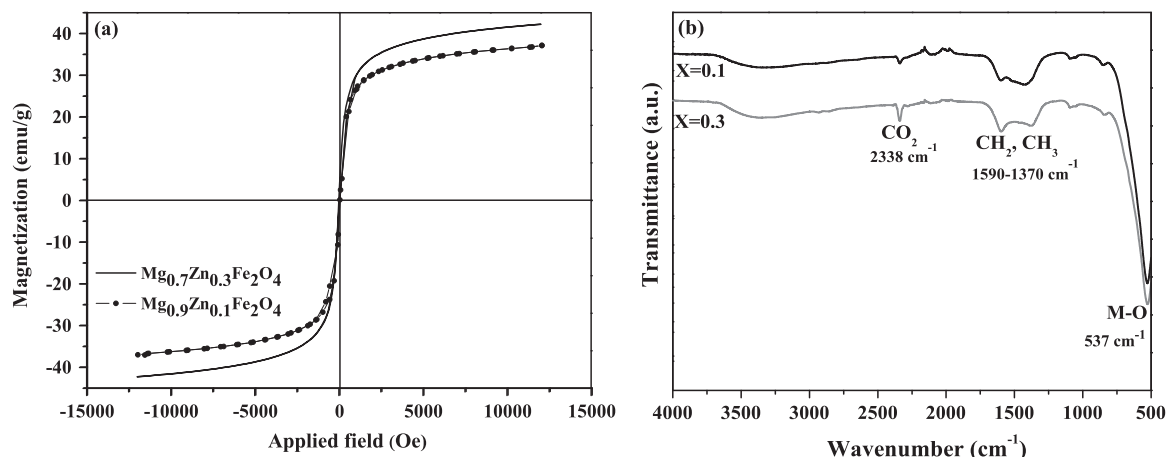


Fig. 2. Hysteresis loops (a) and FT-IR spectra (b) of $Mg_{0.9}Zn_{0.1}Fe_2O_4$ and $Mg_{0.7}Zn_{0.3}Fe_2O_4$ samples.

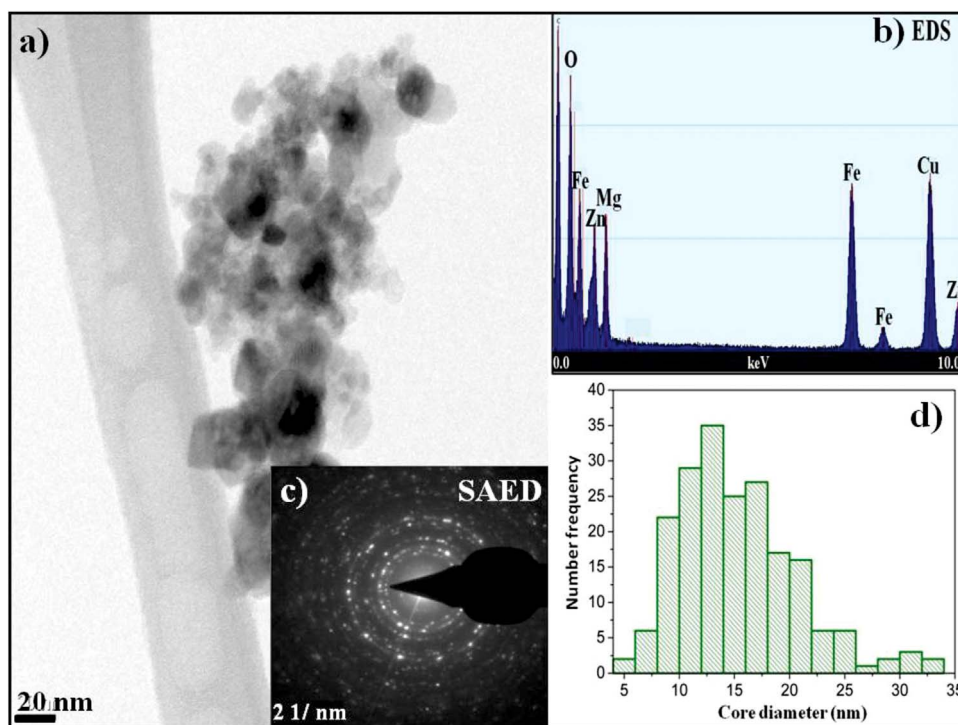


Fig. 3. (a) TEM image, (b) EDS spectrum, (c) SAED and (d) particle size distribution (log-normal shaped) of $Mg_{0.7}Zn_{0.3}Fe_2O_4$ nanoparticles.

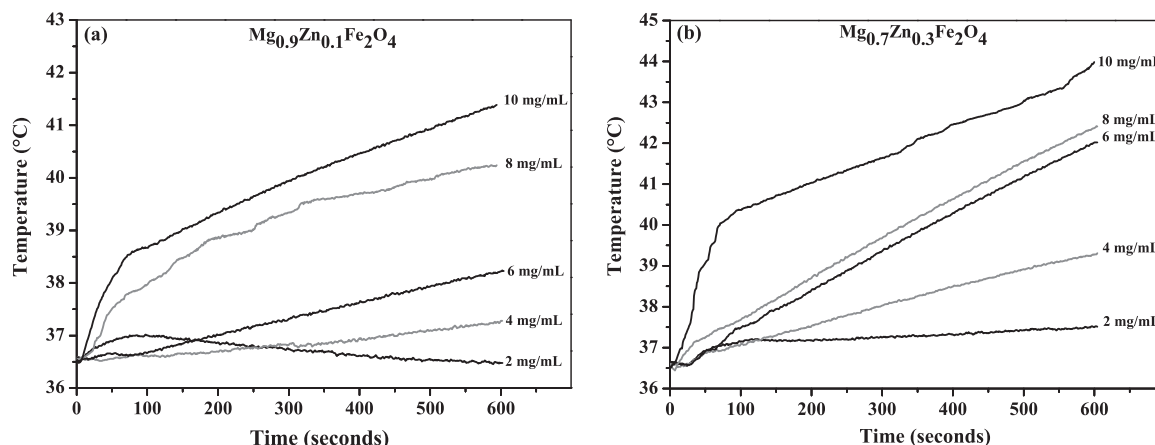


Fig. 4. Heating ability of $Mg_{0.9}Zn_{0.1}Fe_2O_4$ (a) and $Mg_{0.7}Zn_{0.3}Fe_2O_4$ (b) aqueous suspensions (10.2 kA/m, 354 kHz).

Table 2

SAR values of $Mg_{0.9}Zn_{0.1}Fe_2O_4$ and $Mg_{0.7}Zn_{0.3}Fe_2O_4$ nanoparticles.

| $Mg_{0.9}Zn_{0.1}Fe_2O_4$ | | | $Mg_{0.7}Zn_{0.3}Fe_2O_4$ | | |
|---------------------------|-------|-----------|---------------------------|-------|-----------|
| Mass (mg) | dT/dt | SAR (W/g) | Mass (mg) | dT/dt | SAR (W/g) |
| 4.0 | 0.001 | 0.94 | 4.0 | 0.006 | 6.69 |
| 6.0 | 0.002 | 1.67 | 6.0 | 0.010 | 7.04 |
| 8.0 | 0.020 | 10.29 | 8.0 | 0.013 | 6.90 |
| 10.0 | 0.024 | 9.95 | 10.0 | 0.045 | 18.73 |

absorption band located at 537 cm^{-1} indicates the stretching vibrations of M-O bonds (metal-oxygen) corresponding to the A and B sites of the spinel structure [3,13]. Additional adsorption bands were also identified, one corresponding to atmospheric CO_2 (2338 cm^{-1}) and two corresponding to either symmetric or asymmetric stretching vibrations of CH_2 and CH_3 functional groups ($1590\text{--}1370\text{ cm}^{-1}$) from residual ethylene glycol used as reaction medium [17].

An image obtained by TEM, corresponding EDS spectrum, size

distribution and selected area electron diffraction pattern (SAED) of $Mg_{0.7}Zn_{0.3}Fe_2O_4$ particles are shown in Fig. 3. The average diameter of nearly spherical particles was $15 \pm 5.4\text{ nm}$, which is close to that calculated by the Scherrer equation. As observed in this TEM image, nanoparticles are agglomerated, which is due to the presence of strong magnetic interactions, as well as Van der Waals forces and high surface energy [18]. The only elements detected were Fe, Mg, Zn and O.

Fig. 4 shows the heating ability of the selected samples ($Mg_{0.9}Zn_{0.1}Fe_2O_4$ and $Mg_{0.7}Zn_{0.3}Fe_2O_4$), dispersed in deionized water, under the application of an AC magnetic field. In accordance with the M_s values, heating ability increases as the Zn^{2+} content is increased and this effect is due to the increase of M_s , as presented in Table 1. The heating ability of samples show a similar behavior, temperature increases with time, apart from the 2 mg/mL suspension, this is mainly due to the fact that the starting temperature used was $36.5\text{ }^\circ\text{C}$ and, when the quantity of magnetic nanoparticles is $\leq 2\text{ mg/mL}$, the temperature increase is not enough to maintain the starting temperature and the sample tends to lose the initial heat. The heating capacity is better for the Zn content of 0.3 (compared to $Zn=0.1$) and that it only

requires 8 mg/mL to reach 42 °C within 600 s as compared to a particle concentration of 10 mg/mL for the Zn=0.1 case. For the 10 mg/mL sample, there is a two stage effect as observed by the change in slope at about 50 s. This can be explained taking into account that highly concentrated suspensions promote firstly an alignment of particles under the applied magnetic field (first stage) and once this is completed, the normal heating due to the hysteresis loss dominates the process (second stage). In this work, the temperature increase is due to the hysteresis loss as a result of the ferrimagnetic behavior of nanoparticles. The heating ability of $Mg_{0.9}Zn_{0.1}Fe_2O_4$ and $Mg_{0.7}Zn_{0.3}Fe_2O_4$ indicates that these nanoparticles can be adequate materials for hyperthermia applications. The calculated SAR values are within the range of 6.90 and 18.73 W/g (Table 2), which are considerably lower than those reported in the literature [10,19,20]. This may be due to the difference in core size diameter and the parameters of the magnetic field used, particularly amplitude.

4. Conclusions

Magnetic $Mg_{1-x}Zn_xFe_2O_4$ nanoparticles ($x=0.0-0.9$) were successfully synthesized by sol-gel method followed by a heat treatment at 500 °C for 60 min. In all the cases, an inverse spinel crystalline structure was obtained. However, for $x > 0.4$ a secondary phase (ZnO) was detected. The saturation magnetization values increase as the Zn content is increased up to $x \leq 0.4$, while for $x > 0.5$, this value decreases due to the formation of ZnO. The $Mg_{0.9}Zn_{0.1}Fe_2O_4$ and $Mg_{0.7}Zn_{0.3}Fe_2O_4$ nanoparticles showed an average particle size of 15 nm and a near-spherical morphology. The temperature required for hyperthermia applications (42 °C) was reached when aqueous suspensions of 10 mg/mL for $Mg_{0.9}Zn_{0.1}Fe_2O_4$ and suspensions of 8 and 10 mg/mL for $Mg_{0.7}Zn_{0.3}Fe_2O_4$ were used. Specific heat absorption rate increased as the concentration of ferrites in the suspensions was increased. These results indicate that these two selected materials are potential candidates as thermoseeds for magnetic hyperthermia treatment.

Acknowledgements

The authors gratefully acknowledge CONACYT, México for the provision of the Pamela Yajaira Reyes Rodríguez scholarship (335331) and SEP-CONACYT (127815) for the financial support of this research.

References

- [1] R. Ghosh, L. Pradhan, Y.P. Devi, S. Meena, R. Tewari, A. Kumar, S. Sharma, N.S. Gajbhiye, R.K. Vatsa, B.N. Pandey, R.S. Ningthoujam, Induction heating

- studies of Fe_3O_4 magnetic nanoparticles capped with oleic acid and polyethylene glycol for hyperthermia, *J. Mater. Chem.* 21 (2011) 13388–13398.
- [2] N.V. Jadhav, A.I. Prasad, A. Kumar, R. Mishra, S. Dhara, K. Babu, C.L. Prajapat, N.L. Misra, R.S. Ningthoujam, B.N. Pandey, R.K. Vatsa, Synthesis of oleic acid functionalized Fe_3O_4 magnetic nanoparticles and studying their interaction with tumor cells for potential hyperthermia applications, *Colloids Surf. B* 108 (2013) 158–168.
- [3] M.F. da Silva, M. Valente, Magnesium ferrite nanoparticles inserted in a glass matrix—microstructure and magnetic properties, *Mater. Chem. Phys.* 132 (2012) 264–272.
- [4] V.D. Kassabova-Zhetcheva, L.P. Pavlova, B.I. Samuneva, Z.P. Cherkezova-Zheleva, I.G. Mitov, M.T. Mikhov, Characterization of superparamagnetic $Mg_xZn_{1-x}Fe_2O_4$ powders, *Cent. Eur. J. Chem.* 5 (2007) 107–117.
- [5] S. Rahman, K. Nadeem, M.A. Rehman, M. Mumtaz, S. Naeem, I.L. Papst, Structural and magnetic properties of ZnMg-ferrite nanoparticles prepared using the coprecipitation method, *Ceram. Int.* 39 (2013) 5235–5239.
- [6] S. Chhaya, M. Pandya, M. Chhantbar, K. Modi, G. Balda, H. Joshi, Study of substitution limit, structural, bulk magnetic and electrical properties of Ca^{2+} substituted magnesium ferrite, *J. Alloy. Compd.* 377 (2004) 155–161.
- [7] J. Sánchez, D. Cortés-Hernández, J. Escobedo-Bocardo, R. Jasso-Terán, A. Zugasti-Cruz, Bioactive magnetic nanoparticles of Fe–Ga synthesized by sol–gel for their potential use in hyperthermia treatment, *J. Mater. Sci. Mater. Med.* 25 (2014) 2237–2242.
- [8] M. Kallumadil, M. Tada, T. Nakagawa, M. Abe, P. Southern, Q.A. Pankhurst, Suitability of commercial colloids for magnetic hyperthermia, *J. Magn. Magn. Mater.* 321 (2009) 1509–1513.
- [9] R. Ludwig, M. Stapf, S. Dutz, R. Müller, U. Teichgraber, I. Hilger, Structural properties of magnetic nanoparticles determine their heating behavior—An estimation of the in vivo heating potential, *Nanoscale Res.* 9 (2014) 1–10.
- [10] M. Zeisberger, S. Dutz, R. Müller, R. Hergt, N. Matusovitch, H. Bönemann, Metallic cobalt nanoparticles for heating applications, *J. Magn. Magn. Mater.* 311 (2007) 224–227.
- [11] R. Wildeboer, P. Southern, Q. Pankhurst, On the reliable measurement of specific absorption rates and intrinsic loss parameters in magnetic hyperthermia materials, *J. Phys. D* 47 (2014) 495003.
- [12] K. Mohammed, A. Al-Rawas, A. Gismelseed, A. Sellai, H. Widatallah, A. Yousif, M. Elzain, M. Shongwe, Infrared and structural studies of $Mg_{1-x}Zn_xFe_2O_4$ ferrites, *Physica B* 407 (2012) 795–804.
- [13] A. Gismelseed, K. Mohammed, A. Al-Rawas, A. Yousif, H. Widatallah, M. Elzain, Structural and magnetic studies of the Zn-substituted magnesium ferrite chromate, *Hyperfine Interact.* 226 (2014) 57–63.
- [14] B.D. Cullity, S.R. Stock, *Elements of X-ray Diffraction*, Prentice Hall, United States, 2001.
- [15] S. Hajarpour, A.H. Raouf, K. Gheisari, Structural evolution and magnetic properties of nanocrystalline magnesium–zinc soft ferrites synthesized by glycine–nitrate combustion process, *J. Magn. Magn. Mater.* 363 (2014) 21–25.
- [16] S. Khot, N. Shinde, B. Ladgaonkar, B. Kale, S. Watawe, Magnetic and structural properties of magnesium zinc ferrites synthesized at different temperature, *J. Adv. Appl. Sci. Res.* 2 (2011) 460–471.
- [17] H. Asoh, S. Ono, Anodizing of magnesium in amine-ethylene glycol electrolyte, *Mater. Sci. Forum* 419–422 (2003) 957–962.
- [18] S. Sheng-Nan, W. Chao, Z. Zan-Zan, H. Yang-Long, S.S. Venkatraman, X. Zhi-Chuan, Magnetic iron oxide nanoparticles: synthesis and surface coating techniques for biomedical applications, *Chin. Phys.* 23 (2014) 037503.
- [19] S. Dutz, M. Kettering, I. Hilger, R. Muller, M. Zeisberger, Magnetic multicore nanoparticles for hyperthermia—Influence of particle immobilization in tumour tissue on magnetic properties, *Nanotechnology* 22 (2011) 265102.
- [20] M. Ma, Y. Wu, J. Zhou, Y. Sun, Y. Zhang, N. Gu, Size dependence of specific power absorption of Fe_3O_4 particles in AC magnetic field, *J. Magn. Magn. Mater.* 268 (2004) 33–39.